1664 *Chem. Mater.* **2010,** *22,* 1664–1672
DOI:10.1021/cm902899t

CHEMISTRY OF MATERIALS
Article

Adsorption of Harmful Organic Vapors by Flexible Hydrophobic Bis-pyrazolate Based MOFs

S. Galli,*[,†] N. Masciocchi,[†,‡] V. Colombo,[†] A. Maspero,*[,†] G. Palmisano,[†] F. J. López-Garzón,[§] M. Domingo-García,[§] I. Fernández-Morales,[§] E. Barea,*[,§] and J. A. R. Navarro*[,§]

[†]*Dipartimento di Scienze Chimiche e Ambientali, Università dell'Insubria, via Valleggio 11, 22100 Como, Italy,* [‡]*CNISM, UdR Como, via Valleggio 11, 22100 Como, Italy, and* [§]*Departamento de Química Inorgánica, Universidad de Granada, Av. Fuentenueva S/N, 18071 Granada, Spain*

Received September 17, 2009. Revised Manuscript Received January 27, 2010

Highly porous homoleptic Ni(bpb) and Zn(bpb) materials have been obtained by reaction of nickel(II) and zinc(II) salts with the deprotonated form of the 1,4-(4-bispyrazolyl)benzene ligand (H_2bpb). Ab-initio structure solution methods and thermodiffractometry have allowed the determination of their crystal structures, framework flexibility, and thermal stability. The different stereochemical requirements of the Ni(II) and Zn(II) ions induce, in Ni(bpb) and Zn(bpb), rhombic and square channels, respectively, accounting for 57 and 65% of the total cell volume. The two materials feature high adsorption capacities toward small gaseous molecules (N_2 and Ar at 77 K, CO_2 and CH_4 at 273 K), peaking at 22 mmol g^{-1} of N_2 in the case of the zinc(II) derivative, which is reflected by a very large surface area (above 2000 m^2 g^{-1}). The flexibility, size, and hydrophobic nature of their channels are adequate also for the incorporation of organic vapors. In this regard, the adsorption of benzene and cyclohexane has been studied under static conditions at 303 K, while that of thiophene has been investigated in dynamic conditions, by measurement, at 298 K, of the breakthrough curves of a flow of CH_4/CO_2 containing 30 ppm of thiophene. Ni(bpb) and Zn(bpb) are outperforming adsorbents, uptaking up to 0.34 g of thiophene per gram of material. The presence of humidity (60%), which is a major drawback for practical applications of MOFs, does not significantly affect the performance of Ni(bpb) in the removal of thiophene, at variance with Zn(bpb) and HKUST-1, $Cu_3(btc)_2$ (btc = benzene-1,3,5-tricarboxylate), which become ineffective in the presence of moisture. Additional XRPD studies have been performed on benzene-loaded Ni(bpb) samples in order to shed some light on the affinity of this material for aromatic guests.

Introduction

The last years have witnessed a blooming of research interest on the preparation, characterization, and optimization of porous functional materials based on metal ions linked by long organic spacers in three-dimensional networks, with the aim of obtaining outperforming adsorbents.[1,2]

The pioneering work of Yaghi's,[3] Kitagawa's,[4] and Férey's[5] groups has been mainly based on porous metal polycarboxylates possessing remarkable functional properties. Several, chemically and thermally stable, porous metal polycarboxylates have been isolated; yet, the easy hydrolyzability of the metal−carboxylate bonds,[6] or the high affinity for water of coordinatively unsaturated metal centers, are main drawbacks for their practical applications, if they have to compete with classical hydrophobic adsorbents like activated carbons.[7] Polyazolate systems, such as tetrazolate, triazolate, imidazolate, and pyrazolate, offer a closely related stereochemistry to carboxylate and, at the same time, a higher basicity, possibly guaranteeing more robust coordinative bonds.[8] In this regard, the very appealing reports of Long's group[9] on transition metal coordination polymers containing the deprotonated form of 1,4-bis(5-tetrazolyl)-benzene (H_2btb) and 1,4-bis(4-pyrazolyl)benzene (H_2bpb) are indicative of the possibilities that this strategy offers (see Scheme 1).

*Corresponding authors. E-mail: simona.galli@uninsubria.it; angelo.maspero@uninsubria.it; ebaream@ugr.es; jarn@ugr.es.

(1) Long, J. R.; Yaghi, O. M. *Chem. Soc. Rev.* **2009**, *38*, 1213–1214.
(2) (a) Batten, S. R.; Neville, S. M.; Turner, D. R. *Coordination Polymers. Design, Analysis and Application*; RSC Publishing: Cambridge, 2009. (b) Wright, P. A. *Microporous Framework Solids*; RSC Publishing: Cambridge, 2008.
(3) Banerjee, R.; Furukawa, H.; Britt, D.; Knobler, C.; O'Keeffe, M.; Yaghi, O. M. *J. Am. Chem. Soc.* **2009**, *131*, 3875−3877, and references therein.
(4) Noro, S.; Kitagawa, S.; Akutagawa, T.; Nakamura, T. *Prog. Polym. Sci.* **2009**, *34*, 240−279, and references therein.
(5) Férey, G. *Chem. Soc. Rev.* **2008**, *37*, 191−241, and references therein.
(6) Proch, S.; Herrmannsdorfer, J.; Kempe, R.; Kern, C.; Jess, A.; Seyfarth, L.; Senker, J. *Chem.—Eur. J.* **2008**, *14*, 8204–8212.
(7) Britt, D.; Tranchemontagne, D.; Yaghi, O. M. *Proc. Nat. Acad. Sci.* **2008**, *105*, 11623–11627.
(8) See, for example: (a) Park, K. S.; Ni, Z.; Coté, A. P.; Choi, J. Y.; Huang, R.; Uribe-Romo, F. J.; Chae, H. K.; O'Keeffe, M.; Yaghi, O. M. *Proc. Nat. Acad. Sci.* **2006**, *103*, 10186–10191. (b) Biswas, S.; Grzywa, M.; Nayek, H. P.; Dehnen, S.; Senkovska, I.; Kaskel, S.; Volkmer, D. *Dalton Trans.* **2009**, 6487–6495.
(9) (a) Dincă, M.; Yu, A. F.; Long, J. R. *J. Am. Chem. Soc.* **2006**, *128*, 8904–8913. (b) Choi, H. J.; Dincă, M.; Long, J. R. *J. Am. Chem. Soc.* **2008**, *130*, 7848–7850.

 Published on Web 02/09/2010

Scheme 1. Schematic Drawing of the 1,4-Bis(4-pyrazolyl)-benzene (H_2bpb, Left) and 1,4-Bis(4-tetrazolyl)benzene (H_2btb, Right) Molecules

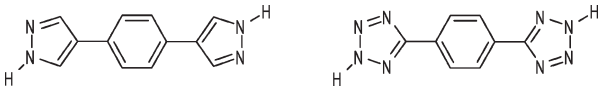

More recent reports have further substantiated the viability of the polyazolate approach to functional porous systems, like MOF-5 analogues exhibiting sensing[10] and catalytic activity.[11] Our recent efforts[12] in tailoring high-yield and cheap syntheses of the H_2btb and H_2bpb polyazoles made it possible to investigate their coordination chemistry toward transition metal ions, in the search for homoleptic porous materials with high chemical and thermal stability, as well as selective adsorptive and catalytic properties.[13] Accordingly, in the following, we will describe the preparation and structural determination by X-ray powder diffraction analysis[14] of the highly porous Ni(bpb) and Zn(bpb) materials, featuring framework flexibility and high thermal stability. Their adsorptive and separation properties (in either static and dynamic conditions) toward gases (N_2, Ar, CH_4, CO_2) and harmful volatile organic compounds (thiophene, benzene, cyclohexane) have been investigated. The effect of the presence of moisture in the vapor adsorption performance, currently a main drawback for MOF's practical applications, has also been evaluated.

Materials and Methods

Physical Measurements. Infrared spectra were recorded on a Shimadzu Prestige-21 instrument. Elemental analyses were carried out on a Perkin-Elmer CHN Analyzer 2400 Series II. Simultaneous TG and DSC analyses were performed in a N_2 stream on a Netzsch STA 409 PC Luxx (heating rate: 10 K min^{-1}).

Gas Adsorption Measurements. Conventional adsorption isotherms were measured using a Micromeritics Tristar 3000 volumetric instrument under continuous adsorption conditions. Brunauer−Emmet−Teller (BET) and Langmuir analyses were used to determine the total specific surface areas for the N_2 and Ar isotherms at 77 K. High pressure adsorption isotherms for CO_2 and CH_4 at 273 K were measured with a homemade volumetric adsorption instrument (University of Granada) equipped with two Baratron absolute pressure transducers (MKS type 627B). Their pressure ranges are 0−133.33 kPa and 0−3333.25 kPa, and the reading accuracy is 0.05% of the usable measurement range. Prior to measurement, powdered samples were heated at 403 K for 12 h and outgassed to 10^{-6} Torr.

Static Vapor Adsorption Studies. The vapor adsorption isotherms for benzene and cyclohexane were acquired at 303 K. All samples were kept for 24 h at each pressure value in order to guarantee that equilibrium was achieved. The amount of vapor adsorbed was measured gravimetrically in a calibrated spring.

Breakthrough Curve Tests. Thiophene removal ability of Zn(bpb), Ni(bpb), and $Cu_3(btc)_2$ (btc = benzene-1,3,5-tricarboxylate)[15] from a He:CO_2:CH_4 gas mixture (about 1:1:2.25 v/v) was examined by a breakthrough experiment using a flow of He:CO_2:CH_4 containing ca. 30 ppm of thiophene. The porous materials (ca. 0.25 g in the form of pellets)[16] were packed into a glass column (0.3 cm inner diameter × 5 cm length). Helium gas was initially purged into the sample column. The column was maintained at 298 K. The gas mixture (100 kPa) was dosed into the column at a flow rate of 30 mL min^{-1}. The presence of humidity after adsorbent activation and the concomitant effect on thiophene removal was also investigated. The relative amounts of the gases passing through the column were monitored on a mass spectrometer gas analysis system (Pfeiffer vacuum) detecting ion peaks at m/z 4 (He), 16 (CH_4), 18 (H_2O), 44 (CO_2), and 84 (thiophene).

Chemicals. All chemicals were of reagent grade and used as commercially obtained. The starting materials 1,4-bis(4-pyrazolyl)-benzene (H_2bpb)[12] and $Cu_3(btc)_2$[17] were prepared following the previously reported procedures.

Synthesis of Ni(bpb). To a solution of $Ni(CH_3COO)_2$ (0.084 g, 0.47 mmol) in acetonitrile (6 mL), solid H_2bpb (0.100 g, 0.47 mmol) was added in one single portion under stirring. The mixture was heated to 60 °C; after 2 min, triethylamine (1.5 mL) was added. The reaction was then kept at 80 °C for 8 h. The dark orange precipitate was filtered off, washed with acetonitrile and methanol, and dried in vacuum. The isolated product is often contaminated by the extremely insoluble H_2bpb ligand, either as the ancillary phase, or trapped in the crystal cavities, much alike terephthalic acid in $Ga(OH)(O_2C-C_6H_4-CO_2)$ and related species of the MIL-53 topology.[18] The unreacted ligand can be eliminated by washing in DMSO (4 mL, at 60 °C for 15 min). In addition, depending on the experimental conditions, the material may contain variable amounts of solvent molecules within the framework cavities. As proved by XRPD, the presence of solvent affects the actual values of the unit cell parameters, yet not the main structural features, with full retention of the space group symmetry. Thus, for sake of simplicity, most of the characterization (elemental analysis, IR spectroscopy, and structure determination) was carried out on a thoroughly evacuated batch, prepared by drying the pure precipitate in vacuum at 150 °C for 4 h. Yield: 70%. IR (nujol): 1581 (s), 1270 (w), 1178 (w), 1144 (m), 1060 (s), 957 (m), 817 (vs), 723 (w). Analysis for $C_{12}H_8NiN_4$ (266.7 g mol^{-1}) calculated: C, 54.00; H, 3.02; N, 20.99. Found: C, 53.70; H, 3.58; N, 20.87.

Benzene loaded samples to be employed in thermodiffractometric analyses (see below) were prepared according to the following procedure: Ni(bpb) was evacuated under mild heating (140 °C) and 10^{-3} mm Hg pressure for about 3 h, then suspended in benzene, and stirred for about 1/2 h. After this treatment, it

(10) Hou, L.; Lin, Y.-Y.; Chen, X.-M. *Inorg. Chem.* **2008**, *47*, 1346–1351.
(11) (a) Lu, Y.; Tonigold, M.; Brendenkötter, B.; Volkmer, D.; Hitzbleck, J.; Langstein, G *Z. Anorg. Allg. Chem.* **2008**, *634*, 2411–2417. (b) Tonigold, M.; Lu, Y.; Brendenkötter, B.; Rieger, B.; Bahnmüller, S.; Hitzbleck, J.; Langstein, G.; Volkmer, D. *Angew. Chem., Int. Ed.* **2009**, *48*, 7546–7550.
(12) Maspero, A.; Galli, S.; Masciocchi, N.; Palmisano, G. *Chem. Lett.* **2008**, *37*, 956–957.
(13) Maspero, A.; Galli, S.; Colombo, V.; Peli, G.; Masciocchi, N.; Stagni, S.; Barea, E.; Navarro, J. A. R. *Inorg. Chim. Acta* **2009**, *362*, 4340–4346.
(14) Masciocchi, N.; Galli, S.; Sironi, A. *Comm. Inorg. Chem.* **2005**, *26*, 1–37.
(15) Chui, S. S.; Lo, S. M.; Charmant, J. P.; Orpen, A. G.; Williams, I. D. *Science* **1999**, *283*, 1148–1150.
(16) The pellets were obtained by pressing the original powder up to 7 tons cm^{-2}. The resulting disks were ground over a 1 mm sieve. The adsorptive properties and XRPD patterns were checked indicating that they are not modified after the pellet formation.
(17) Schlichte, K.; Kratzke, T.; Kaskel, S. *Microporous Mesoporous Mater.* **2004**, *73*, 81–88.
(18) Volkringer, C.; Loiseau, T.; Guillou, N.; Férey, G.; Elkaïm, E.; Vimont, A. *Dalton Trans.* **2009**, 2241−2249, and references therein.

was filtered and immediately sent to the powder diffractometer for evaluation of its desorption kinetics.

Synthesis of Zn(bpb). Solid H_2bpb (0.100 g, 0.47 mmol) was added to a solution of $Zn(ClO_4)_2 \cdot 6H_2O$ (0.177 g, 0.47 mmol) in benzonitrile (6 mL). The mixture was heated at 70 °C; after 2 min, triethylamine (1.5 mL) was added. The reaction was then kept at 150 °C for 4 h. After cooling the reaction vessel down to RT, the white precipitate was filtered off, washed with benzonitrile, methanol, and dried in vacuum at RT to afford the final product. Yield: 90%. IR (nujol): 1584 (s), 1350 (s), 1286 (m), 1174 (m), 1133 (s), 1056 (vs), 956 (s), 826 (vs), 723 (w). Analysis for $C_{12}H_8N_4Zn \cdot 2PhCN$ (479.86 g mol^{-1}) calculated: C, 65.08; H, 3.78; N, 17.51. Found: C, 65.13; H, 3.90; N, 17.47. Depending on the experimental conditions, the polycrystalline material is recovered with variable amounts of solvent molecules hosted in the crystal lattice. For the sake of coherence, most of the characterization (elemental analysis, IR spectroscopy and structure determination) was carried out on the batch showing the highest degree of crystallinity—incidentally, the one possessing two molecules of PhCN per formula unit. A thoroughly evacuated batch can be prepared by drying the washed precipitate in vacuum at 150 °C for 4 h.

X-ray Powder Diffraction Analysis. Powdered, microcrystalline samples of M(bpb) (M = Ni, Zn) were gently ground in an agate mortar, then deposited in the hollow of an aluminum sample holder (equipped with a zero-background plate). Diffraction data were collected with overnight scans in the 5−105° 2θ range on a Bruker AXS D8 Advance diffractometer, equipped with a linear position-sensitive Lynxeye detector, primary beam Soller slits, and Ni-filtered Cu−Kα radiation (λ = 1.5418 Å). Generator setting: 40 kV, 40 mA. Figure S1 (of the Supporting Information) contains the low-angle portion of the collected diffraction data, highlighting the relative differences and the less-than-ideal crystallinity of the samples, showing anisotropic peak broadening. A standard peak search, followed by indexing with TOPAS,[19] allowed the detection of the approximate unit cell parameters: orthorhombic *I*, a = 6.75 Å, b = 22.78 Å, c = 13.45 Å, V = 2069.4 $Å^3$, and GOF = 35.5 for Ni(bpb); tetragonal *P*, a = 13.28 Å, c = 7.26 Å, V = 1280 $Å^3$, and GOF = 12.4 for Zn(bpb). The space groups *Imma*, for Ni(bpb), and $P4_2/mmc$, for Zn(bpb), were assigned on the basis of the systematic absences conditions and were later confirmed by Le Bail refinements.

Structure solutions were performed by the simulated annealing technique, as implemented in TOPAS, using for bpb a rigid, idealized model and for Zn(bpb) adding a rigid (and disordered) PhCN molecule. The final refinements were carried out by the Rietveld method, maintaining the rigid bodies introduced at the structure solution stage. In both cases, the background was modeled by a polynomial function; anisotropic broadening, in the form of spherical harmonics, was used to define the peak widths. Peak shapes and an estimation of the coherent scattering domains (not grains sizes, as normally measurable by DLS experiments or SEM micrographs) were determined by the fundamental parameters approach, allowing for the Lorentzian broadening in the convolutory approach.[20] Peak shape and width parameters were calibrated using the NIST Standard Reference Material SRM 660a LaB_6. One refinable isotropic thermal parameter was assigned to the metal atoms, augmented by 2.0 $Å^2$ for lighter atoms. The final Rietveld refinement plots are shown in Figure S2 (of the Supporting Information).

(19) *TOPAS*, version 3.0, Bruker AXS: Karlsruhe, Germany, 2005.
(20) (a) Cheary, R. W.; Coelho, A. *J. Appl. Crystallogr.* **1998**, *31*, 851–861. (b) Cheary, R. W.; Coelho, A. *J. Appl. Crystallogr.* **1998**, *31*, 862–868.

Crystal data for Ni(bpb). $C_{12}H_8N_4Ni$, fw = 266.92 g mol^{-1}; orthorhombic, *Imma*, a = 6.7655(15) Å, b = 22.7353(3) Å, c = 13.4648(1) Å; V = 2071.1(4) $Å^3$; Z = 4; ρ_{calc} = 0.856 g cm^{-3}; $F(000)$ = 544; μ(CuKα) = 12.6 cm^{-1}. R_p, R_{wp}, and R_{Bragg} 0.034, 0.058, and 0.026, respectively, for 28 parameters.

Crystal data for Zn(bpb)·2PhCN. $C_{26}H_{18}N_6Zn$, fw = 479.86 g mol^{-1}; tetragonal, $P4_2/mmc$, a = 13.2657(7) Å, c = 7.2474(11) Å; V = 1275.4(3) $Å^3$; Z = 2; ρ_{calc} = 1.250 g cm^{-3}; $F(000)$ = 492; μ(CuKα) = 15.2 cm^{-1}. R_p, R_{wp}, and R_{Bragg} 0.059, 0.074, and 0.015, respectively, for 33 parameters.

Crystallographic data (excluding structure factors) for the structures reported in this paper have been deposited with the Cambridge Crystallographic Data Centre as supplementary publication nos. CCDC 742072−742073. Copies of the data can be obtained free of charge on application to CCDC, 12 Union Road, Cambridge CB2 1EZ, UK (fax +44 1223 336 033; e-mail deposit@ccdc.cam.ac.uk).

Thermodiffractometric Studies. Thermodiffractometric experiments were performed on solvated M(bpb) materials, to highlight the response of the two frameworks to desolvation. The experiments were carried out in air[21] from 298 K up to the loss of crystallinity using a custom-made sample heater, assembled by Officina Elettrotecnica di Tenno, Ponte Arche, Italy. Powdered microcrystalline samples of M(bpb) (M = Ni, Zn) were deposited in the hollow of an aluminum sample holder; diffractograms at different temperatures (with steps of 20 K) were recorded in a significant low-angle 2θ range. Le Bail refinements were used to derive the lattice constants, later employed in the determination of the thermal properties. By means of the same apparatus, another set of experiments was performed on benzene-loaded Ni(bpb): consecutive diffractograms were acquired in isothermal conditions at 298, 323, and 348 K to characterize the evolution of the system. The data were treated by the Le Bail refinement method to derive the corresponding unit cell parameters. Furthermore, estimation of the integrated area by single peak modeling of the low angle section allowed the estimation of the kinetic parameters by applying the Avrami model.[22]

Results and Discussion

Synthesis. Ni(bpb) is obtained in the form of a dark orange precipitate when a solution of $Ni(CH_3COO)_2$ is refluxed with H_2bpb in acetonitrile and in the presence of a base, such as triethylamine. Zn(bpb) is isolated as a white product by reacting $Zn(ClO_4)_2$ with H_2bpb in benzonitrile and, again, in the presence of triethylamine. In both cases, analytical, spectroscopic and, above all, XRPD evidences suggested that samples obtained in different syntheses had slightly distinct stoichiometries and lattice metrics (vide infra), as if a variable amount of solvent had remained trapped in what were later found to be highly porous coordination polymers.

(21) Thermal treatments of our materials have been performed in air (TXRPD) and in N_2 atmosphere, using the standard equipment available in our laboratories. While this difference must be considered important when O_2 can induce side reactions, decomposition, etc., in our cases the thermal analyses were performed to study the desorption of solvent (DMSO, PhCN, and water) molecules, which are not affected by the presence of a pure gas, or of a mixture of gases, as long as their inert behaviour is guaranteed. Obviously, decomposition of the framework under oxidizing conditions may occur at lower temperatures than under N_2.
(22) Avrami, M. *J. Chem. Phys.* **1941**, *9*, 177−184, and references therein.

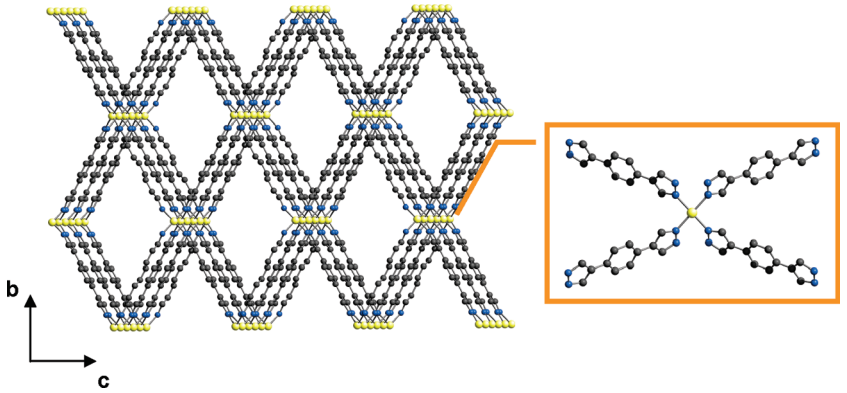

Figure 1. Schematic drawing of the crystal structure of Ni(bpb) viewed approximately down **a**. Carbon, gray; hydrogen, light gray; nitrogen, blue; nickel, yellow. While details of the metal center stereochemistry are lost in this view, the large voids (accounting for nearly 57% of the total volume), generated by the rhomboic disposition of the bridging ligands, are easily appreciated. The insert shows the square planar stereochemistry at the nickel(II) ions. Hydrogen atoms have been omitted for clarity.

Crystal Structure of Ni(bpb). This compound crystallizes in the orthorhombic *Imma* space group; the asymmetric unit contains one Ni(II) ion (2/*m* symmetry positions, Wyckoff site *c*) and one bpb ligand located about an inversion center. Each metal center is coordinated, in square-planar stereochemistry, by four nitrogen atoms of four distinct bpb moieties [Ni−N 1.973(1) Å; N−Ni−N 84.6(3) and 95.4(3)°]. This feature has already been found in simpler analogues, such as the nickel imidazolate,[23] and, more pertinently, pyrazolate species.[24] With each pyrazolic end, the bpb ligands bridge, in the common exobidentate mode, Ni···Ni contacts of 3.37 Å[25] (*a*/2), generating linear and parallel chains of Ni(II) ions. The chains, further connected, and maintained nearly 13.2 Å apart, by the bpb moieties, eventually generate a 3D network, in which large cavities of rhomboic shape (see Figure 1) represent about the 57% of the crystal volume (as calculated by Platon[26]). Not surprisingly, the estimated bulk density of Ni(bpb) is 0.86 g cm^{-3}.

As already pointed out in the experimental section, and as later substantiated, depending on the thermal history and on the actual reaction conditions, the structure may host variable amounts of solvent molecules, with significant deformation of the overall lattice metrics, but neither of the symmetry nor of the topology. Similar versatility and flexibility properties have been recently observed in some metal hydroxo-terephthalates, such as the Al/Cr/Fe/Ga-based MIL-53 frameworks, showing occasional symmetry changes upon guest adsorption or release.[27,28]

Crystal Structure of Zn(bpb). This crystal phase is tetragonal, space group $P4_2/mmc$; the asymmetric unit contains one crystallographically independent Zn(II) ion (−4*m*2 position, Wyckoff site *e*) and one bpb molecule (*mmm* symmetry position, Wyckoff site *d*). The tetrahedrally coordinated metal centers (Zn−N 2.04 Å; N−Zn−N 108−112°) are kept 3.62 Å (*c*/2) apart by the bpb moieties along linear chains parallel to **c**. The chains are further connected into a 3D framework by the bpb spacers, decorating the walls of the unit cell and generating square channels with 13.2 Å edges, running parallel to **c** (Figure 2).

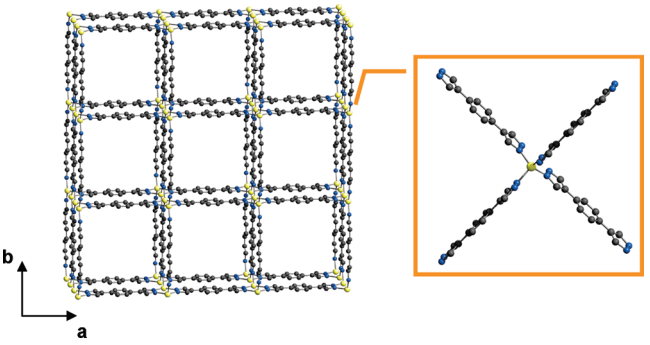

Figure 2. Schematic drawing of the crystal structure of Zn(bpb) viewed approximately down **c**. Carbon, gray; hydrogen, light gray; nitrogen, blue; zinc, yellow. While details of the metal center stereochemistry are lost in this view, the large voids (accounting for nearly 65% of the total volume), generated by the square disposition of the bridging ligands, can be appreciated. The insert shows the tetrahedral stereochemistry at the zinc(II) ions. Hydrogen atoms have been omitted for clarity.

Therefore, apart from the symmetry lowering induced by the partial organization of the trapped solvent molecules observed in Long's Co(bpb),[9b] the zinc and cobalt species are isostructural, as expected for transition metal ions favoring tetrahedral stereochemistry. *In the freshly prepared samples*, analytical and structural data coherently suggest the presence of variable amounts of PhCN, ranging from a Zn(bpb)·2PhCN formulation, down to a pure Zn(bpb) phase, once evacuation is achieved upon heating the solvated phase. Upon desolvation, the large cavities account for about 65%[26] of the crystal volume, with a calculated density of only 0.71 g cm^{-3}, and can host infinitely long cylinders nearly 6.6 Å wide. The density value, and the slightly higher one observed for Ni(bpb),

(23) Masciocchi, N.; Castelli, F.; Forster, P. M.; Tafoya, M. M.; Cheetham, A. K. *Inorg. Chem.* **2003**, *42*, 6147–6152.
(24) Masciocchi, N.; Ardizzoia, G. A.; Brenna, S.; LaMonica, G.; Maspero, A.; Galli, S.; Sironi, A. *Inorg. Chem.* **2002**, *41*, 6080–6090.
(25) The intermetallic distance in the two Ni(pz)$_2$ polymorphs is ca. 3.48 Å.
(26) Spek, A. L. *J. Appl. Crystallogr.* **2003**, *36*, 7–13.
(27) Chaplais, G.; Simon-Masseron, A.; Porcher, F.; Lecomte, C.; Bazer-Bachi, D.; Bats, N.; Patarin, J. *Phys. Chem. Chem. Phys.* **2009**, *11*, 5241–5245.
(28) Ferey, G.; Serre, C. *Chem. Soc. Rev.* **2009**, *38*, 1380−1399, and references therein.

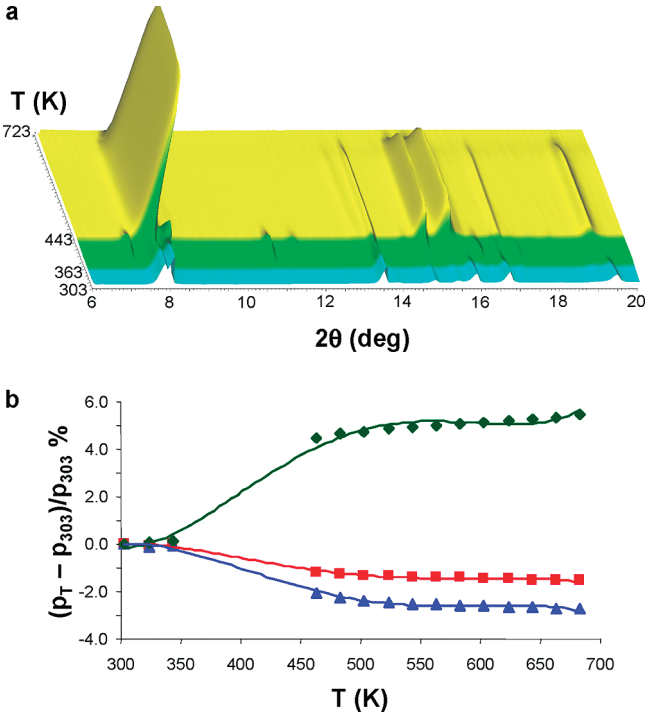

Figure 3. (a) Variable temperature X-ray diffractograms acquired on solvated Ni(bpb) in the 303−723 K temperature range. The cyan and yellow intervals denote, respectively, the solvated and the empty phase; the light green region indicates the transition between the two phases. (b) Variation of the unit cell parameters of Ni(bpb) (p_T) normalized to the correspondent 303 K values (p_{303}) as a function of the temperature. *a*, red squares; *b*, blue triangles; *c*, green rhombi. The reported lines have the only scope of guiding the eye. The Le Bail refinement of the temperature range drawn in green in the upper part was not possible, as no lattice periodicity values could be derived for this transient phase.

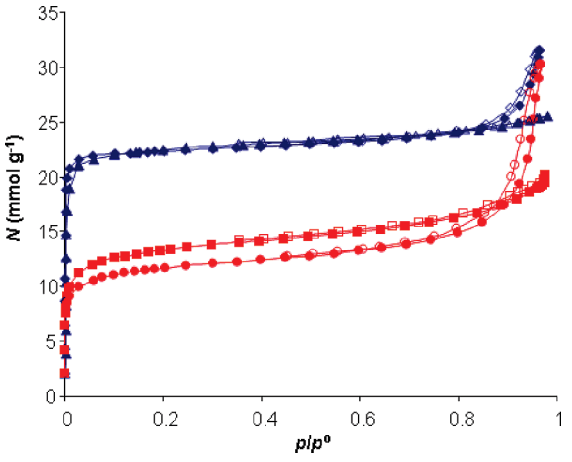

Figure 4. Ni(bpb): N_2 (red circles) and Ar (red squares) adsorption isotherms at 77 K. Zn(bpb): N_2 (blue diamonds) and Ar (blue triangles) adsorption isotherms at 77 K. Open symbols denote desorption.

are in agreement with the exceptionally high surface area and gas and vapor adsorption performances reported below.

Thermal Behavior. The thermal behavior of compounds M(bpb) (M = Ni, Zn) was investigated by coupling simultaneous thermal analyses (STA, simultaneous TG and DSC) to in situ variable temperature X-ray powder diffraction (TXRPD).

Thermal Behavior of Ni(bpb). The simultaneous thermal analysis performed on a DMSO solvated batch of Ni(bpb) showed a smooth and continuous mass loss from 323 to 733 K, the temperature at which decomposition starts. The observed mass loss has been interpreted as the evolution of the clathrated solvent. The TXRPD experiments (Figure 3) carried out in air on the *very same batch* of Ni(bpb) further substantiated the STA observations: up to 323 K, only the fully solvated (A) phase is present; further heating in the 363−443 K temperature range induces a smooth and continuous solvent loss, during which a still unindexed material (with broad diffraction peaks) is formed; after that, a single new phase (B) is formed, from which the residual solvent molecules continue to be lost until decomposition. While preserving the unit cell symmetry, the A → B process brings about definite changes in the positions and intensities of the XRPD peaks. A structureless Le Bail refinement of the TXRPD data was carried out in the temperature ranges in which pure (A or B) phases were present. The results show that, on passing from the A (303 K) to the B species (463 K), **a** is the cell axis less affected by the thermal treatment (Figure 3b): this is somehow expected, as **a** is associated with the chains propagation direction, where collinear metal atoms are kept at a nearly constant separation by the bridging pyrazolate rings. On the contrary, **b** and **c**, defining the rhomboic disposition of the 1-D chains, undergo higher, and inversely correlated, variations. Specifically, while **b** decreases, **c** increases, the two events globally resulting in a breathing of the 3D framework promoted by guest release, namely inflating the rhomboic channels with a concomitant unit cell volume increment of about 1.0%. Further heating of the B phase brings about moderate cell parameters variations in the same direction as those just described, with a modest cell volume shrinking (0.5%).

Interestingly, different preparations typically afforded materials with different XRPD traces, all of them referring to the same *Imma* structure, but lying on intermediate points in the (solvent promoted) deformation path. RT measurements of Ni(bpb) batches with different degrees of solvation allowed to observe unit cell axes variations up to about 20% of their (lowest) values. Again, **a** is only marginally affected, while **b** and **c** show significant and inversely correlated variations (Figure S3 of the Supporting Information).

Thermal Behavior of Zn(bpb). Also Zn(bpb) room temperature XRPD traces of different preparations differ among each other, although to a lesser extent. Figure S4 (of the Supporting Information) shows the powder diffraction pattern of the sample recovered with the highest, even less than ideal, crystallinity, whose structural details have been discussed above, compared with that of a batch possessing an even lower degree of crystallinity, as witnessed by the definitely broadened peaks. As evident from Figure S5, depicting its thermodiffractogram, Zn(bpb) is rather stiff during desolvation and does not show the extreme flexibility of the Ni(II) analogue. Given its structural features, one can easily interpret this behavior by the stereochemical rigidity of the ZnN_4 tetrahedron,

Table 1. Summary of Gas and Vapor Adsorption Capacities of Ni(bpb) and Zn(bpb) Materials[c]

Compound	BET ($m^2\ g^{-1}$)	N_2 (mmol g^{-1})	Ar (mmol g^{-1})	CO_2 (mmol g^{-1})	CH_4 (mmol g^{-1})	benzene (mmol g^{-1})	cyclohexane (mmol g^{-1})	pore V_{ads}[a] ($cm^3\ g^{-1}$)	pore V_{cryst}[b] ($cm^3\ g^{-1}$)
Ni(bpb)	1600	12.0	13.7	10.0	3.7	5.8	6.5	0.38	0.67
Zn(bpb)	2200	22.5	22.7	9.1	2.4	3.8	4.7	0.71	0.92

[a] Accessible pore volume obtained from N_2 adsorption isotherms (*t*-plot). [b] Pore volume calculated from crystal structures. [c] These values were obtained from the adsorption isotherms of N_2 and Ar (77 K), CO_2 and CH_4 (273 K), and benzene and cyclohexane (303 K). N_2 adsorption capacities correspond to a relative pressure of 0.3, CO_2 and CH_4 capacities were taken at 3000 kPa, and benzene and cyclohexane values correspond to a relative pressure of 1.

and of the tetragonal lattice as a whole. This observation is in contrast with what shown by the isostructural (orthorhombic and monoclinic) Co(bpb) materials: in both cases, thermal treatment[9b,29] or catalytic tests[29] induce not yet interpreted, profound structural changes.

Adsorption Properties. *Gas Adsorption*. Two different sets of experiments have been performed on the M(bpb) species (M = Ni, Zn): (i) in order to evaluate their potential use for gas separation and storage of small gaseous molecules, the gas adsorption properties of the activated M(bpb) solids have been essayed toward Ar and N_2 at 77 K and CH_4 and CO_2 at 273 K; (ii) aiming at determining their suitability for the separation and removal of harmful vapors, the adsorption of organic vapors in static (benzene, cyclohexane) or dynamic (thiophene) conditions (in both dry and humid environments) has been studied.

Figure 4 shows the adsorption isotherms of Ar and N_2 at 77 K for the two materials. Both nickel and zinc derivatives display the typical behavior of highly porous crystalline MOFs. Indeed, they both exhibit type I adsorption isotherms with a sharp knee at low relative pressures ($p/p_0 \sim 0.01$, corresponding to the filling of the porous structure), followed by a *plateau*, suggesting that the permanent porosity of the samples is mainly composed of micropores, of rather uniform size. Additionally, the presence of a (type H1) hysteresis loop in the N_2 isotherms at relative pressures above 0.8 is indicative of textural mesoporosity arising from interparticle mesopores (voids).[30] This is indeed in line with the apparent average particle sizes (approximated by the coherent scattering domains) determined by diffraction methods, typically lying in the 50−200 nm range. The highly porous nature of both materials is also manifested by their large specific surface areas, with values of ca. 1600 and 2200 $m^2\ g^{-1}$ for Ni(bpb) and Zn(bpb), respectively, as obtained by the BET method (Table 1). The Zn(bpb) system exhibits a large gas storage capacity amounting to 22.5 mmol g^{-1} of N_2 and Ar at 77 K, which is indicative of a very high accessibility of its microporous structure (0.71 $cm^3\ g^{-1}$, as calculated from the *t*-plot method, closely matching the value obtained from the structural model) (Table 1). It should be noted that, in contrast to the Co(bpb) species,[9] the closely related Zn(bpb) material does not exhibit steps in the low pressure region. As anticipated, Co(bpb) and

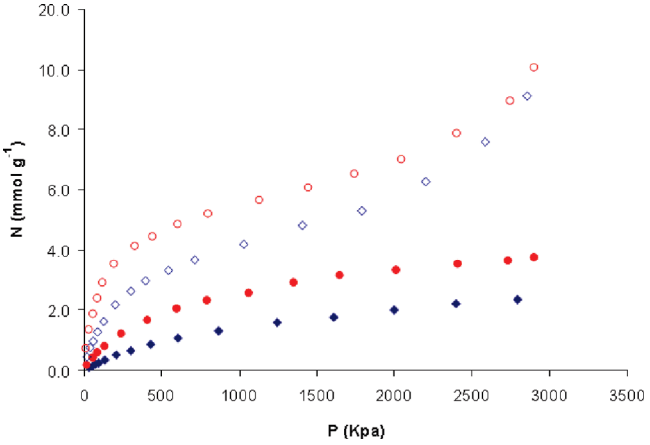

Figure 5. High pressure CO_2 (open symbols) and CH_4 (full symbols) adsorption isotherms at 273 K for Ni(bpb) (red circles) and Zn(bpb) (blue diamonds).

Zn(bpb) are isomorphous species (apart from negligible symmetry lowering due to the organization of the clathrated solvent molecules in the former); thus, we tentatively attribute the absence of detectable steps in the gas sorption curves of Zn(bpb) to its *extreme* rigidity (as witnessed by our TXRPD analysis), i.e. to the difficulty of distorting the T_d geometry of Zn(II) ions (but not that of Co(II) ones) toward D_{2d}. In the case of Ni(bpb), the storage capacity (12 mmol g^{-1} of N_2; 13.7 mmol g^{-1} of Ar) significantly diminishes. In this regard, it should be noted that pore volume (0.38 $cm^3\ g^{-1}$), as calculated from the *t*-plot, is significantly lower than the crystallographic pore volume; it is possible that, due to its remarkable flexibility, a narrow pore form of this material is present at low temperatures, which we cannot trap.

The high pressure adsorption isotherms of CO_2 and CH_4 at 273 K for the Zn(bpb) and Ni(bpb) materials, measured up to 3000 kPa (Figure 5), show, in the low pressure range, a smooth increase in the adsorbed amount and the appearance of a sigmodial shape at high pressures, which indicates a relatively weak interaction of these guest molecules within the cavities of the adsorbent. This is a consequence of the large size of the pore channels which lead to a behavior that closely resembles that of the bulk fluid, as already found in highly porous MOF's, e.g. MOF-177 and IRMOF-1.[31] In contrast to the adsorption isotherms of N_2 and Ar at 77 K, the Ni(bpb) material outperforms, by a factor of 2, the adsorption capacity of Zn(bpb) in the whole pressure range (up to 2850 kPa),

(29) Lu, Y.; Tonigold, M.; Bredenkötter, B.; Volkmer, D.; Hitzbleck, J.; Langstein, G. *Z. Anorg. Allg. Chem.* **2008**, 2411–2417.
(30) Rouquerol, F.; Rouquerol, J.; Singh, K. S. S. *Adsorption by powders and porous solids*; Academic Press: New York, 1999.
(31) Millward, A. R.; Yaghi, O. M. *J. Am. Chem. Soc.* **2005**, *127*, 17998–17999.

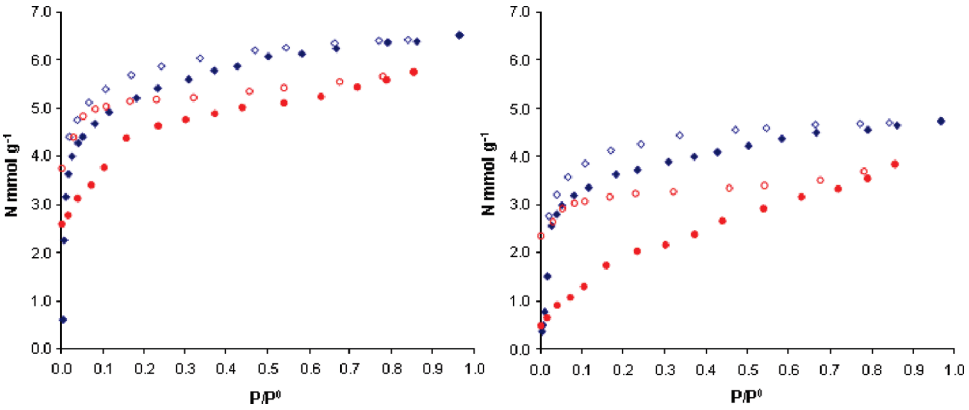

Figure 6. Vapor adsorption−desorption isotherms of benzene (red circles) and cyclohexane (blue diamonds) at 303 K for Ni(bpb) (left) and Zn(bpb) (right). Open symbols denote the desorption branch.

thus suggesting that the narrower size and adaptive nature of the pores of the Ni(II) derivative is a fundamental issue.[32] For both materials, the adsorption capacity for CO_2, peaking up to 10 mmol g^{-1} at 2850 kPa for Ni(bpb) (Table 1), closely approaches that exhibited by the best performing MOF materials MIL-53[32] and IR-MOFs-1,-3,-6, and -11[31] and might be of interest for the storage of this greenhouse gas. The storage capacities of CH_4 at 273 K are much smaller, with a maximum value of 3.75 mmol g^{-1} for Ni(bpb) (Table 1). The lower adsorption capacity of CH_4 compared to CO_2 can be attributed to the fact that methane adsorption is carried out in supercritical conditions, with concomitant weaker adsorbate−adsorbate and adsorbate−adsorbent interactions for CH_4 in comparison to CO_2. All together, these results suggest that the interaction of small gaseous molecules like CO_2 and CH_4 is weak, thus requiring, in spite of the large surface areas exhibited by these materials, high pressures in order to achieve significant storage capacities at temperatures close to ambient conditions.

Organic Vapor Adsorption. At variance with the above results, the interaction of the Ni(bpb) and Zn(bpb) systems with organic vapors (benzene, cyclohexane, thiophene) appears to be very strong in both static and dynamic conditions. Figure 6 shows the adsorption isotherms of the two materials toward benzene and cyclohexane at 303 K. In the case of cyclohexane, it can be appreciated the formation of quasireversible type I isotherms exhibiting high storage capacities of 6.5 and 4.7 mmol g^{-1} for Ni(bpb) and Zn(bpb), respectively (Table 1). These values are comparable to those exhibited by $[Zn(bdc)(ted)_{0.5}]$, which possesses a similar pore volume and similar adsorption capacity toward organic vapors at 298 K, namely 6.2 mmol g^{-1} of benzene and 5 mmol g^{-1} of cyclohexane.[33] In the case of benzene, adsorption proceeds in a stepwise fashion, with an abrupt rise in the adsorption capacity in the low pressure range, particularly evident in the case of Ni(bpb). These observations possibly indicate strong interactions of the guest molecules with primary binding sites and, for Ni(bpb), a stepwise behavior, in which guest incorporation or release is responsible for a significant breathing effect of the porous flexible structure (see below).[32] By contrast, the desorption branch follows a type I isotherm. A significant part of the adsorbed benzene (3.8 mmol g^{-1} for Ni(bpb) and 2.3 mmol g^{-1} for Zn(bpb)) (Table 1) is irreversibly captured inside the porous network giving rise to the formation of an irreversible adsorption isotherm with a pronounced hysteretic loop. This parallels our observations on the presence of residual solvents (DMSO or PhCN) after the isolation of the raw materials. On the other hand, in the case of Ni(bpb), the volume of adsorbed benzene (0.5 mL g^{-1}) and cyclohexane (0.7 mL g^{-1}) fits well with the calculated crystallographic pore volume (0.67 mL g^{-1}), which implies the complete filling of the pores during the adsorption process and confirms the optimal interactions among these adsorbates and the pore walls. In contrast, in Zn(bpb), the pore filling is lower than expected from crystallographic data (pore volume, 0.92 mL g^{-1}) as adsorbed benzene and cyclohexane accounts only for 0.3 and 0.5 mL g^{-1}, respectively. These results are probably indicative that, in this case, slightly weaker interactions of the organic molecules with the framework walls are taking place as a consequence of the stiffer nature of the coordination network and the larger size of the pores.

In view of the affinity of these systems for aromatic vapors, we realized that these systems might be of interest for the selective removal of harmful organic vapors from natural gas or air purification purposes. In this regard, it should be noted that although the well-known $Cu_3(btc)_2$ [7] material has been shown to behave as an excellent adsorbent of tetrahydrothiophene, it is ineffective in the presence of humidity as a consequence of irreversible water coordination to the open metal sites. This feature of MOFs with open metal sites is a main drawback for their application if they have to compete with classical hydrophobic adsorbents like activated carbons. With the aim of studying the behavior of our novel pyrazolate based systems, we have evaluated their performance in the removal of thiophene (ca. 30 ppm) from a He:CH_4:CO_2 1:2.25:1 (v:v) flow in both dry and humid conditions. The dynamic adsorption process of thiophene in the

(32) Llewellyn, P. L.; Bourrelly, S.; Serre, C.; Filinchuk, Y.; Férey, G. *Angew. Chem., Int. Ed.* **2006**, *45*, 7751–7754.
(33) Lee, J. Y.; Olson, D. H.; Pan, L.; Emge, T. J.; Li, J. *Adv. Funct. Mater.* **2007**, *17*, 1255–1262.

absence of moisture has been studied by measurement of a breakthrough curve at 298 K. The results show that these systems are suited for the selective incorporation of thiophene in dynamic conditions (Figure 7a).

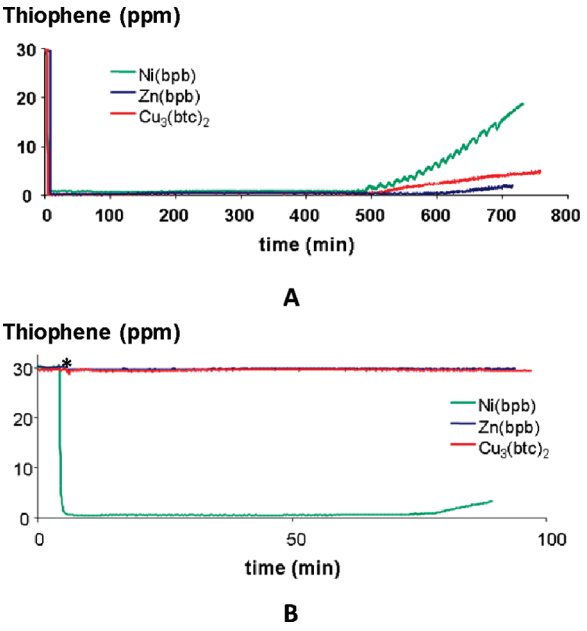

Figure 7. (A) Breakthrough curves for a He:CH_4:CO_2 1:2.25:1 (v/v) gas mixture containing 30 ppm of thiophene flowed through a column packed with activated Ni(bpb) (green), Zn(bpb) (blue), or $Cu_3(btc)_2$ (red). (B) Effect of the presence of humidity on the performance of thiophene removal. Ni(bpb), Zn(bpb), or $Cu_3(btc)_2$ have been exposed to open air for 72 h prior to usage, and the flowed gas mixture used contained 60% humidity. The asterisk indicates the time in which the gas mixture is flowed through the MOF bed.

The maximum adsorbed vapor amounts reach 0.30 and 0.34 g thiophene g^{-1} for Ni(bpb) and Zn(bpb), respectively, and are fully comparable with those of the best performing MOF-type material known to date for adsorption of organo-sulphur compounds, namely $Cu_3(btc)_2$.[7] Remarkably, exposition for 72 h to open air (298 K, 60% humidity) of the Ni(bpb), Zn(bpb), and $Cu_3(btc)_2$ materials prior to the breakthrough tests, as well as incorporation of humidity (60%) in the gas flow stream still permits the incorporation of thiophene by the nonactivated Ni(bpb) (0.060 g thiophene g^{-1}, Figure 7b). By contrast, Zn(bpb) and $Cu_3(btc)_2$ materials are totally inefficient for this purpose in humid conditions (Figure 7b). Thus, thanks to the synergic effects of different structural, stereochemical, and energetic features (the flexibility of its framework, the hydrophobic nature of the 1D channels, the probable interactions of the thiophene *S*-donor atoms with the Ni centers and the insensitive nature of the metal coordination sphere to moisture and hydrolysis), Ni(bpb) appears to be very promising for the incorporation of a MOF in a gas purification device (Scheme 2). By contrast, the activity for thiophene removal under humid conditions is dramatically lowered in the case of Zn(bpb) and $Cu_3(btc)_2$: this can be attributed to framework rigidity in Zn(bpb) and to the loss of the coordinatively unsaturated metal centers in $Cu_3(btc)_2$, which does not permit the direct interaction of the thiophene *S*-donor atoms with the M(II) ions.

Structural Deformations upon Vapor Adsorption and Removal. XRPD studies of the Ni(bpb) material loaded with benzene have been performed in order to further highlight the structural changes that take place upon

Scheme 2. Schematic Drawing of Thiophene Interaction with the [$Cu_3(btc)_2$] (Left) and [Ni(bpb)] (Right) Host Frameworks in Both Dry and Humid Conditions[a]

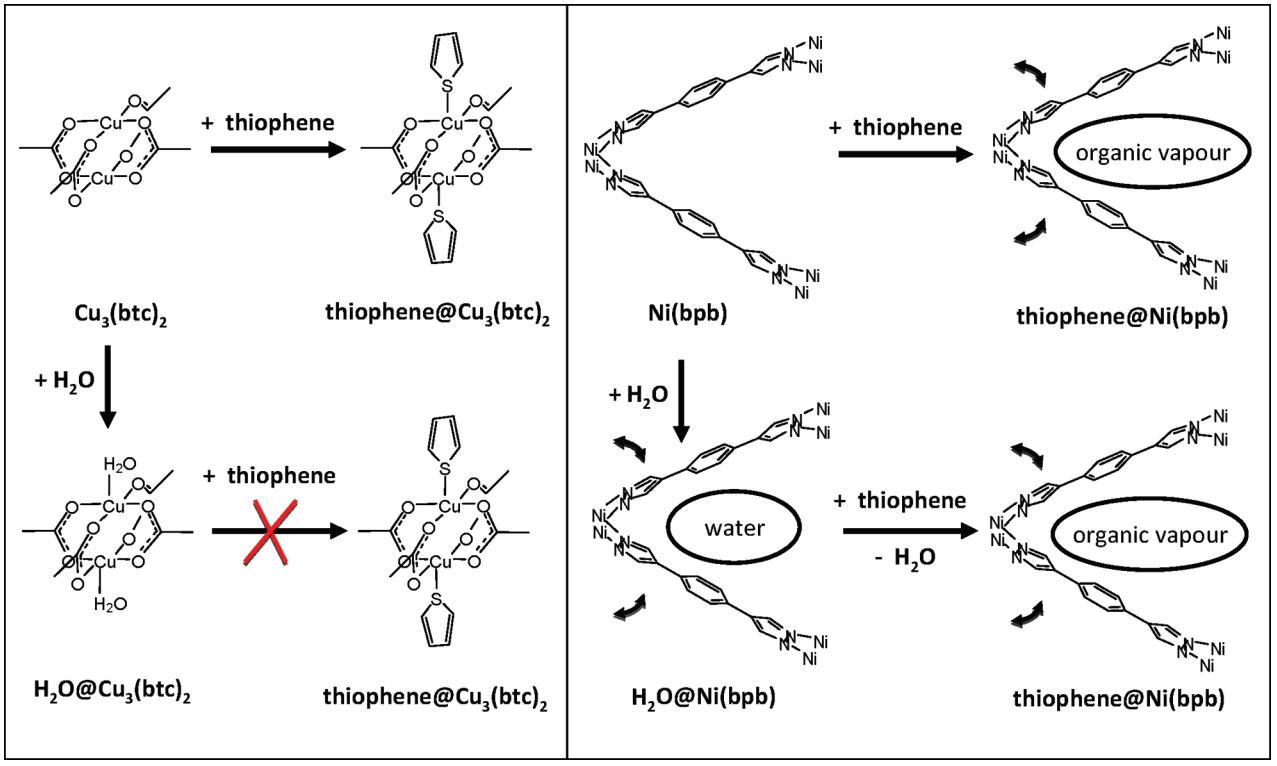

[a] In the case of [$Cu_3(btc)_2$], the blocking effect of coordinated water molecules on thiophene uptake is highlighted.

Table 2. Unit Cell Parameters of the Ni(bpb) Material Loaded with Different Guest Molecules at 298 K[a]

compound	space group	*a*, Å	*b*, Å	*c*, Å	*V*, Å^3	*b*/*c*
Ni(bpb)	*Imma*	6.76	22.73	13.46	2071	1.69
DMSO@Ni(bpb)	*Imma*	6.84	23.24	12.95	2060	1.79
benzene@Ni(bpb)	*Imma*	6.67	22.58	13.29	2004	1.70

[a] The effective uncertainty values of the lattice parameters of the solvated phases, measured at room temperature and upon heating (in air) on transient (unstable) materials, are expected to be larger than the e.s.d.'s determined by least squares methods and Le Bail refinements (a few thousands of angstroms) and estimated to be in the 0.01−0.02 Å range.

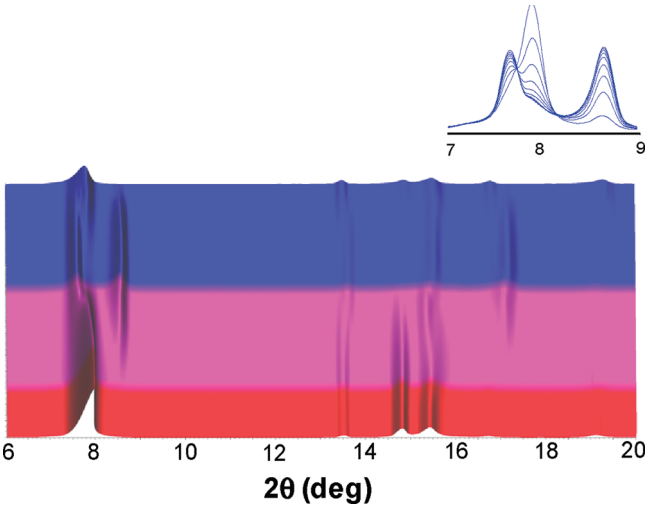

Figure 8. Evolution of the XRPD trace for Ni(bpb) loaded with benzene during desorption under isothermal conditions, at 298, 323, and 348 K. Blue, lilac, and red traces represent isothermal measurements at 298, 323, and 348 K, respectively. Each full set of data took about 3 h (approximately 5 min per single pattern). The insert shows the low-angle regions from which clear isosbestic-like points can be observed, requiring the absence of intermediate phases during transformation.

incorporation and release of guest molecules. XRPD measurements on the benzene@Ni(bpb) material performed at 298 K are indicative that the freshly loaded material shows the same space group and related cell metrics as the pristine Ni(bpb) (Table 2). XRPD traces acquired at 298 K, under strictly isothermal conditions, are indicative of a dynamic desorption process which is accompanied with remarkable changes of the rhomboic channels dimensions (Figure 8), much alike Férey's MIL-53 species[32] and its congeners. The evolution of benzene stops approximately after 40 min of air exposure: the XRPD traces asymptotically reach an equilibrium state with some benzene still occluded in the pores, as confirmed by the benzene adsorption experiments described above. This transformation *is not mediated by any intermediate phase*, since isosbestic-like points can be easily seen for overlapping (some increasing and some decreasing) peaks. Using these data, the Avrami model[22] for solid-state reaction kinetics has been applied, giving a phenomenological time-exponent of 1.5, thus discarding the occurrence of 3D random nucleation. Progressive exposure of the material to higher temperatures, namely 323 K and, eventually, 348 K overnight, fully restores the dimensions of the channels as in the empty Ni(bpb) material (Figure S6 of the Supporting Information), which is maintained also upon cooling the sample back to room temperature. These results are also in agreement with previous ones obtained by TXRPD on the DMSO loaded Ni(bpb) samples (see above). However, it seems that DMSO induces larger distortions compared to benzene (Table 2) which might be related to the nonplanar nature of the former guest.[34]

Conclusions

The recent reports on the structure and porosity of a few metal btb and bpb 3D networks[9] and the availability of these ligands by new efficient syntheses[12,13] have prompted us to investigate novel coordination polymers with late transition metals. We have here presented the synthesis and full characterization of the Ni(II) and Zn(II) species with the long bpb spacer, which show permanent porosity and a certain degree of flexibility. In this regard, the (thermo)diffractometric measurements have quantitatively addressed the nature and the extent of the lattice flexibility featured by the isostructural frameworks crystallizing in the *Imma* and closely related space groups, as discussed in a very recent contribution to this field.[27]

More importantly, our adsorption studies confirmed the formation of porous systems with highly accessible channels, particularly adequate for the selective incorporation of organic vapors. In this regard, the moisture insensitive nature of Ni(bpb), coupled to its framework flexibility and to its very high thermal stability, was shown to be highly suitable for thiophene removal from CO_2/CH_4 mixtures *even in the presence of humidity*, thus overcoming the still unsolved problems raised by classical carboxylate-based MOF's in real practical applications, such as their incorporation in filters for air and gas purification processes.

Work can be anticipated in extending the isoreticular approach to other polyazolate systems with longer aromatic spacers, or with a different number of donor sites, aiming at the formation of porous networks with high flexibility and possessing high chemical inertness and thermal stability.

Acknowledgment. This work was supported by the Italian MIUR (PRIN2006: "Materiali Ibridi Metallo-Organici Multifunzionali con Leganti Poliazotati"), Fondazione CARIPLO (Project 2007-5117), FP7-EU (nanoMOF), Spanish MCINN (CTQ2008-00037/PPQ), and Junta de Andalucía. E.B. thanks Spanish MICINN for a "Ramon y Cajal" contract. We thank the reviewers for helpful suggestions.

Supporting Information Available: Figures S1−S7: Comparison of raw XRPD and Rietveld refinement plots for the M(bpb) compounds; quantification of Ni(bpb) framework flexibility; TXRPD plots for Zn(bpb) and Ni(bpb) loaded with benzene. Crystallographic data for Ni(bpb) and Zn(bpb) as CIF files. This material is available free of charge via the Internet at http://pubs.acs.org.

(34) Whether the coordination of DMSO to Ni(II) ions occurs either through the oxygen or through the sulfur atoms could not be experimentally assessed. A search in the Cambridge Structural Database (version September 2009) demonstrates that, for first row transition metal ions, O-linkage isomers are preferred, though S-linkage ones are also known.